Robust RFID-Based Respiration Monitoring in Dynamic Environments

Yanni Yang, Jiannong Cao, *Fellow, IEEE*, and Yanwen Wang, *Member, IEEE*

Abstract—Respiration monitoring (RM) is crucial for tracking various health problems. Recently, RFID has been widely employed for lightweight and low-cost RM. However, existing RFID-based RM systems are designed for static environments where no people move around the monitored person. While, in practice, most environments are dynamic with people moving nearby, which introduces dynamic multipath signals and significantly distorts the respiration signal, leading to inaccurate RM. In this paper, we aim to realize accurate RFID-based RM in dynamic environments. Our observations show that multipath signals can result in a similar pattern to respiration, which leads to mis-detection of apnea and inaccurate respiration rate estimation. To address this issue, we first measure the respiration anomaly in the signal spectrogram to detect apnea. Second, we successfully remove the multipath effect for respiration rate estimation inspired by the intrinsic features of human respiration. Specifically, compared with people's moving pattern, respiration pattern is regular and periodic. By transforming a normal respiration cycle into a matched filter, real respiration cycles can be extracted from the noisy RFID signal, which can be applied to estimate the respiration rate via peak detection scheme. The experiments show that our system achieves the average error of 4.2% and $0.51\ bpm$ for apnea detection and respiration rate estimation in dynamic environments, respectively.

Index Terms—Respiration monitoring, RFID, dynamic environment, multipath effect

1 INTRODUCTION

RESPIRATION state is not only an important indicator for reflecting the respiratory conditions but also highly related to the overall homeostatic control for human health. Respiration state of a human shows early signs for many diseases, e.g., sleep apnea [1], hypoxia [2], and chronic obstructive pulmonary disease (COPD) [3]. In addition, monitoring respiration state can help to prevent the disease deterioration for patients in a sensitive and accurate way [4]. Therefore, accurate and continuous respiration monitoring (RM) is highly demanded for people suffering from various health problems.

However, traditional respiration monitoring (RM) approaches that use wearable devices are either cumbersome or intrusive to users. For example, the chest belt/nostril sensors, which are tightly bound on the chest/nose, could make users feel uncomfortable when being monitored. Recently, radio frequency (RF) signals have shown great potential for non-intrusive RM, which aims to release people from wearing bulky sensors [5], [6], [7], [8], [9], [10], [11]. Among different RF technologies, RFID has been well investigated for RM due to the small, lightweight, and flexible properties of passive RFID tags [12], [13], [14], [15], which offer a non-intrusive way for RM by simply attaching RFID tags on the chest. Meanwhile, RFID tags are cost-effective (0.1-0.2 USD per tag) and can be applied for large-scale deployment. The intuition of RFID-based RM is that the tiny periodic chest movement during breathing can be captured by tracking the movement of the tag on the chest.

RFID technology has many advantages over other RF technologies for RM. First, the WiFi-based method is hard to support multi-person RM. Although some works implement WiFi-based multi-person RM [5], [7], they require prior knowledge of the number of persons. In addition, WiFi-based methods fail to match the respiration rate to each corresponding person. However, thanks to the standard EPC communication protocol, multi-person RM can be achieved and separated via the unique ID of tags attached on different persons chests. Compared with the radar-based methods, which require specialized RF devices [10], [11], the commodity RFID devices are widely used in the market. Thus, using RFID can provide a more pervasive RM for public use.

However, current RFID-based RM systems can only monitor the person in a relatively static environment where no people move around so that the tiny chest movement caused by human respiration can be correctly measured [12], [13], [14], [16], [17]. As depicted in Fig. 1a, a person is monitored in a static environment, and the measured respiration signal from the RFID tag shows a clear periodic respiration pattern. However, in dynamic environments with people moving nearby, as shown in Fig. 1b, the measured respiration signal becomes noisy. This is because the surrounding people incur dynamic multipath signals, which are superimposed with the desired line-of-sight (LOS) respiration signal of the monitored person. As a result, the respiration pattern in the RFID signal would be distorted, which

- *Yanni Yang and Jiannong Cao are with the Department of Computing, The Hong Kong Polytechnic University, Hong Kong. E-mail: yan-ni.yang@connect.polyu.hk, jiannong.cao@polyu.edu.hk.*
- *Yanwen Wang is with the College of Electrical and Information Engineering, Hunan University, Changsha 410082, China, and also with the Department of Computing, The Hong Kong Polytechnic University, Hong Kong. E-mail: wangyw@hnu.edu.cn.*

Manuscript received 2 Mar. 2021; revised 5 July 2021; accepted 17 Aug. 2021. Date of publication 0 . 0000; date of current version 0 . 0000.
(Corresponding author: Yanwen Wang.)
Digital Object Identifier no. 10.1109/TMC.2021.3106954

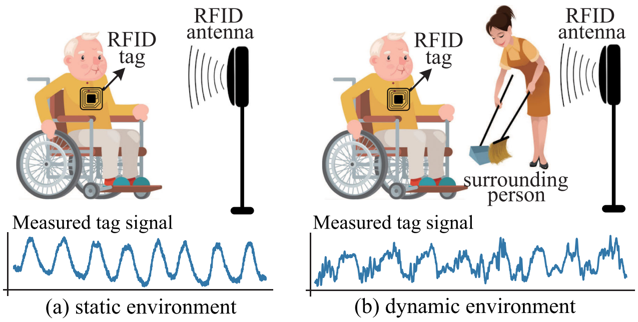

Fig. 1. Respiration monitoring in the static and dynamic environments. The signal in the dynamic environment suffers from many noises compared with that in the static environment.

could result in inaccurate RM results. In this work, we propose RM-Dynamic, which aims to remove the effect of multipath signals in dynamic environments for realizing robust RFID-based RM with accurate apnea detection and respiration rate estimation.

To achieve this goal, *we first elaborate how the dynamic multipath signals from moving people affect the respiration signal of the monitored person.* Previous works only model the effect of multipath signals based on the signal path change [18], [19]. However, the change of the RFID signal (e.g., signal phase) incurred by the multipath signals is subject to many factors, e.g., the antenna radiation range, people's moving area, and movement pattern. In our work, we perform a detailed investigation of these effects on the RFID signal in terms of the signal phase. In specific, we find that multipath signals caused by moving people can introduce a similar pattern in the signal phase as that resulting from the chest movement during respiration. As a result, multipath signals could distort the original respiration signal with both high-frequency noises and fake respiration cycles, which lead to inaccurate respiration state measurements.

The second task is to remove the effect of multipath signals for accurate apnea detection. In dynamic environments, the surrounding movements can result in the missing detection of apnea, which is a respiratory anomaly of sudden cessation of breathing. This is because the phase of multipath signals may occasionally exhibit a sinusoidal wave, which shares a similar pattern to the respiration signal, even if when the monitored person stops breathing with no chest movement. This would misguide that the monitored person is still breathing and lead to the missing diagnosis of apnea. To address this issue, we investigate the spectrogram of respiration and multipath signals in the frequency domain. In specific, we compare the dominance of their frequency components within the respiration frequency range. For the respiration signal, the most dominant frequency components fall into the respiration frequency range. In contrast, the frequency components of multipath signals are less dominant in the respiration frequency range. With this in mind, we define a respiration-dominance index (RDI) which counts the number of dominant frequencies within the respiration frequency range in the spectrogram. The measured RDI is compared with a reference RDI obtained from the normal respiration signal to differentiate the apnea out of the multipath signals.

The third task is to remove the effect of multipath signals for accurate respiration rate estimation. To achieve this, we borrow insights from the inherent features of the human respiration pattern. Human-beings have a regular and periodic respiration rhythm which is unique and diverse among individuals [20]. Compared with the irregular patterns of people's moving, respiration presents a regular and rhythmic pattern. This inspires us to transform the real respiration cycle into a matched filter to extract the desired respiration signal mixed with the multipath signals. After filtering, there will be repetitive peaks in the matched filter output which match the corresponding respiration cycles. By detecting the peaks, we can estimate the respiration rate.

Note that the performance of the matched filter depends on the shape of the real respiration cycle. However, respiration patterns are diverse for different persons and may change along with time. To obtain optimal performance of the matched filter, we first propose a cycle-averaging method to obtain the respiration cycle template for each user. Then, we design a respiration template update method to automatically adapt to the change of respiration pattern.

In sum, our work makes the following contributions:

- To the best of our knowledge, RM-Dynamic is the first work to study the problem of RFID-based RM in dynamic environments. We can accurately estimate the respiration state when people move in the vicinity of the monitored person.
- We perform a detailed analysis on how the multipath signals from surrounding people's movements affect the respiration signal. We investigate the key factors that affect the pattern of multipath signals, which facilitates the understanding of the RFID multipath effect in this field.
- Based on the intrinsic features of respiration pattern, we analyze the signal's spectrogram for accurate apnea detection and design a matched filter for accurate respiration rate estimation. Experimental results show that our system achieves similar performance on apnea detection (4.2% error) and respiration rate estimation ($0.51\ bpm$ error) in dynamic environments compared with those in static environments.

2 RFID-Based Respiration Monitoring and the Multipath Effect

In this section, we introduce how the RFID signal phase is affected by both the respiration activity and the multipath signals incurred by surrounding people's movements.

2.1 Phase of the Respiration Signal

To interrogate an RFID tag, the RFID reader first sends out a continuous wave (CW) to activate the tag. After being powered up, the tag modulates its information on the CW and reflects it back to the reader. The commodity RFID reader can then extract and output the low-level data of the RFID signal. In our work, we use the RFID signal phase to measure the respiration state, since the signal phase is more sensitive to the minute chest movement during breathing [12].

To thoroughly understand the RFID signal phase, we interpret it from the aspects of both signal voltage and signal traveling distance. First, we refer to the phasor space, as shown in Fig. 2a, to show how the signal phase is measured

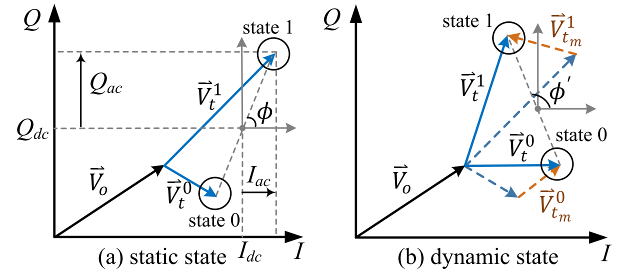

Fig. 2. Demodulated voltage of the tag signal received by RFID reader.

from the signal voltage. When the RFID reader receives the tag backscattered signal, it is converted into the baseband signal $\vec{V}$, which can be represented as follows [21]:

$$\vec{V} = \vec{V_o} + \vec{V_t^i};\ \vec{V_o} = \vec{V}_{leak} + \vec{V}_{scatter}. \tag{1}$$

$\vec{V_o}$ is decided by the reader transmitter to receiver leakage $\vec{V}_{leak}$ and scattering $\vec{V}_{scatter}$ from the environment. $\vec{V_t^i}$ is the voltage of the tag backscattered signal. $\vec{V_t^i}$ changes with the state of the tag chip (i = state 0 or 1). State 1 and state 0 refer to the matching and mismatching states between the input impedance of the tag antenna and the tag chip [22], respectively. After removing the DC component in $\vec{V}$, the signal phase ϕ is calculated as follows:

$$\phi = ang(\vec{V_t^1} - \vec{V_t^0}) = arctan\left(\frac{Q_{ac}}{I_{ac}}\right), \tag{2}$$

where Q_{ac} and I_{ac} refer to the AC quadrature and in-phase components, respectively. When the tag moves along with the chest movement while breathing, $\vec{V_t^i}$ will rotate back and forth, resulting in a periodic change of the signal phase.

Second, the signal phase can also be expressed as a function of the signal traveling distance d as follows:

$$\phi = \left\{2\pi \cdot \frac{d}{\lambda}\right\} \bmod\ 2\pi, \tag{3}$$

where λ is the signal wavelength. During respiration, with the RFID tag attached on the chest and facing to the antenna directly, Equ. (3) becomes

$$\phi = \left\{2\pi \cdot \frac{2[d_0 + d_r(t)]}{\lambda}\right\} \bmod\ 2\pi, \tag{4}$$

where d_0 is the initial distance between the tag and the antenna. $d_r(t)$ is a sinusoidal function which describes the chest movement. As the chest moves forward and backward periodically, the signal phase exhibits a periodic pattern accordingly with valleys and peaks indicating the expansion and contraction of the chest, respectively.

2.2 Phase of Multipath Signals

In RFID-based RM systems, the LOS signal between the tag and antenna is used for extracting the respiration pattern [9], [12], [13], [14]. While, in practice, many reflectors in the environment, e.g., surrounding people and furniture, could bring multipath signals. As shown in Fig. 3, the static object and moving person bring different multiple signals. Such multipath signals can be superimposed with the LOS signal at the receiver, which greatly affects the signal phase.

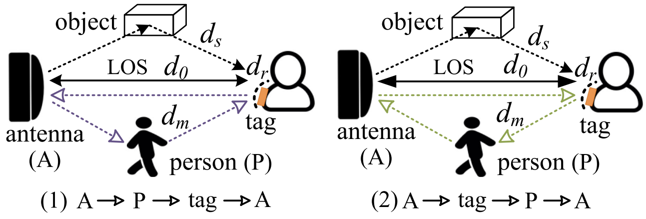

Fig. 3. Propagation path of multipath signals from moving person.

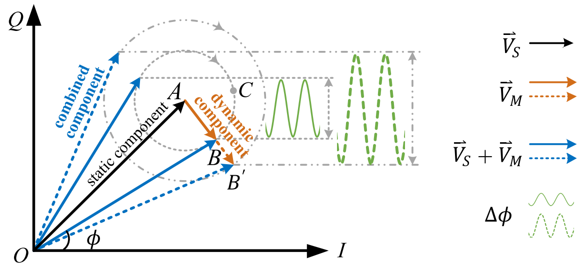

Fig. 4. Effect of dynamic multipath signals on the signal phase.

When surrounding people move nearby the tag, the multipath signals' voltage is added on the received signal, and the tag signal phase ϕ can be expressed as

$$\phi = ang\left[\underbrace{\sum_{s=1}^{S}(\vec{V}^1_{t_s} - \vec{V}^0_{t_s})}_{\vec{V}_S} + \underbrace{\sum_{m=1}^{M}(\vec{V}^1_{t_m} - \vec{V}^0_{t_m})}_{\vec{V}_M}\right], \tag{5}$$

where $\vec{V}^{1,0}_{t_s}$ is the voltage of static components, including the static LOS signal and static multipath signals. $\vec{V}^{1,0}_{t_m}$ refers to the voltage of dynamic multipath signals. S and M are the total numbers of static signals and dynamic multipath signals in the environment, respectively.

In the phasor space, suppose the tag is attached on a static object, $\vec{OA}$ in Fig. 4 represents the sum of static components, i.e., $\vec{V}_S$ in Equ. (5). When people move around the tag, the dynamic component $\vec{V}_M$, i.e., $\vec{AB}$ in Fig. 4, will rotate from 0 to 2π. The measured phase is denoted by the combined component $\vec{OB}$. In consequence, the combined phase is jointly affected by $|\vec{V}_M|$ and $\angle\vec{V}_M$ (the angle between $\vec{V}_M$ and I-axis). When people move nearby the tag, the strength (length) of $|\vec{V}_M|$ varies, e.g., $|\vec{V}_M|$ increases from $\vec{AB}$ to $\vec{AB'}$. Meanwhile, $\angle\vec{V}_M$ may also change accordingly, e.g., $\angle\vec{V}_M$ decreases when $\vec{AB}$ rotates to $\vec{AC}$. Then the combined signal phase will change accordingly. Therefore, in the following sections, we will study how surrounding people's movements affect the signal phase from the views of $|\vec{V}_M|$ and $\angle\vec{V}_M$.

2.2.1 Effect of $|\vec{V}_M|$

By investigating the effect of surrounding people's movements on $|\vec{V}_M|$, we can compare the magnitude of phase changes incurred by respiration with those from people's moving. To achieve this, we look into the propagation paths of multipath signals. As shown in Fig. 3, multipath signals primarily propagate in two ways [18]: (1) antenna → person → tag → antenna; (2) antenna → tag → person → antenna.

In propagation way (1), the moving person affects the downlink of multipath signals, i.e., [antenna → person →

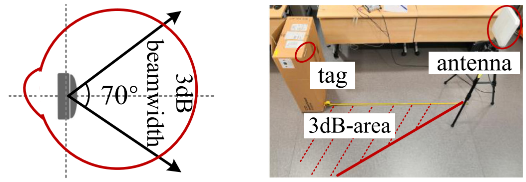

(a) antenna radiation area (b) setting of antenna & tag

Fig. 5. Illustration of RFID antenna radiation range and $3\ dB$ beamwith.

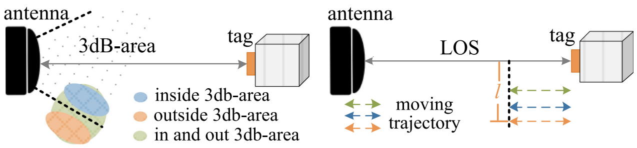

(a) move around antenna (b) move around tag

Fig. 6. Moving area and trajectory of the surrounding person.

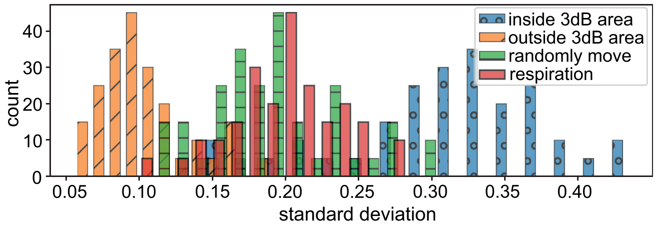

Fig. 7. Distribution of standard deviation of the signal phase with moving people moving in different areas.

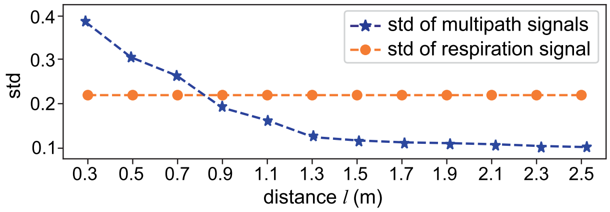

Fig. 8. Standard deviation of signal phase for different distances l.

tag]. At this point, $|\vec{V}_M|$ mainly depends on the strength of multipath signals which are dominated by the reflection of the moving person from the antenna to tag. As a result, the person's moving area around the antenna is the key factor of $|\vec{V}_M|$. The RFID antenna is usually directional and has an effective radiation area, inside which a $3\ dB$ beamwidth area (denoted as $3\ dB$-area) exits. Fig. 5a shows a $3\ dB$-area for the Laird antenna [23]. The area inside the red circle is the effective radiation range, and the inner area segmented by the two black arrows is the $3\ dB$-area. When the person moves inside the $3\ dB$-area, more multipath signals are reflected by the person with a stronger signal magnitude, and vice versa.

To see the effect of people's moving area around the antenna on the signal phase, we attach an RFID tag on a stationary box and place the antenna $1.5\ m$ away facing to the tag straightly, as shown in Fig. 5b. A red line is drawn on the ground as the $3\ dB$ beamwidth boundary. Volunteers are asked to walk insides, outside, and randomly in and out of the 3dB-area without blocking the LOS path, as shown in Fig. 6a. Since volunteers move closer to the antenna, different moving distances to the tag, i.e., the effect from the uplink signal, introduce limited impact to the signal phase and can be ignored.

To compare the phase changes caused by the respiration activity and those brought by the surrounding movements in different areas, we employ the standard deviation (std) of the signal phase, which can serve as a good indicator to measure the variations in the signal. The larger the std is, the larger phase changes are incurred by the movement. The distributions of the std of the signal phase for people moving inside, outside, and randomly in and out of the $3\ dB$-area are shown in Fig. 7. We also depict the std of the signal phase merely caused by the respiration activity. From Fig. 7, we obtain the following observations: (1) The std of the signal phase when people move inside $3\ dB$-area is generally larger than that of outside the $3\ dB$-area. This is because the movements inside the $3\ dB$-area can result in a larger $|\vec{V}_M|$. (2) The std distributions of the random moving and respiration overlap each other, showing that the multipath signals of moving people have similar effects on the phase changes compared with the respiration activity. Therefore, surrounding people's movements could bring comparable phase changes as the respiration activity.

For propagation way (2), the moving person mainly affects the uplink of multipath signals, i.e., [tag $\rightarrow$ person $\rightarrow$ antenna]. In this case, $|\vec{V}_M|$ is mainly decided by the strength of multipath signals which are dominated by the reflection of the moving person from the tag to antenna. Therefore, the distance between the moving person and tag becomes the key factor for the phase changes. To observe this effect, we ask a volunteer to walk along a straight line nearby the tag with different distances l to the LOS line, as shown in Fig. 6b. Since the volunteer mainly moves around the tag and is relatively far from the antenna, different moving areas towards the antenna, i.e., the effect from the downlink signal, cause little effect on the signal phase and can be neglected. The average std of the signal phase for different l is given in Fig. 8. The std first falls sharply and then decreases smoothly along with the increase of l. Thus, the effect of multipath signals when the moving person is far from the monitored person is limited. However, if the person moves close to the monitored person, multipath signals could affect the respiration pattern and should be carefully removed.

2.2.2 Effect of $\angle\vec{V}_M$

The effect of $\angle\vec{V}_M$ can be revealed from the moving pattern of surrounding people. We analyze the people's moving pattern from two aspects. First, the torso movement can result in two possible changes of $\angle\vec{V}_M$, i.e., rotating clockwise and counterclockwise, which causes the increase and decrease of $\angle\vec{V}_M$. Second, people's limbs could swing periodically during walking, which could lead to a rhythmic change of $\angle\vec{V}_M$ whose frequency is similar to the limb swing frequency within the range of $1.5-2.5\ Hz$ [24]. Thus, people's moving also brings relatively high-frequency components in the signal phase compared with the human respiration frequency range of $0.17-0.55\ Hz$ [25].

To show the effect of surrounding people's torso and limb movements, we fix the tag on a stationary box and ask a person to walk from the antenna towards the tag, then stop for a while, and finally walk backward. The measured signal phase is depicted in Fig. 9. The general increasing and decreasing trend (highlighted by yellow dashed arrows) are mainly caused by the torso moving from the

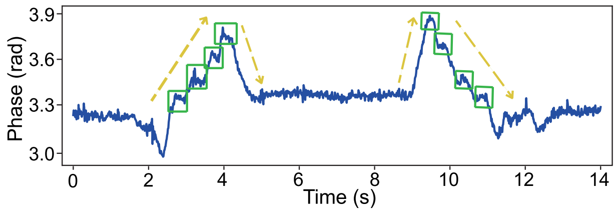

Fig. 9. Phase of multipath signals caused by a person walking by.

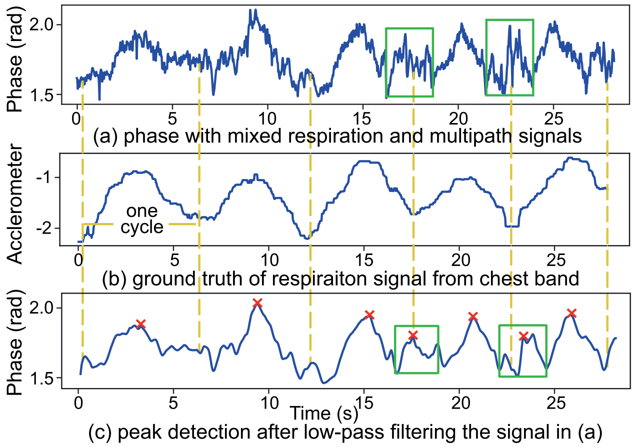

Fig. 10. Multipath mixed respiration signal, ground truth respiration signal, and peak detection result.

antenna to the tag side. Meanwhile, the small peaks in the green rectangular are due to the periodic limb movements during walking. The effect from the high-frequency limb movements can be removed by a low pass filter. However, the general increasing and decreasing trend in Fig. 9 may be mis-detected as fake respiration cycles, which should be eliminated from the signal phase.

In sum, based on the analysis of $|\vec{V}_M|$ and $\angle\vec{V}_M$, the multipath signals of moving people could distort the respiration signal with comparable magnitude changes of the signal phase, which include both high-frequency noises and fake respiration cycles.

2.3 Respiration Signal Mixed With Multipath Signals

To investigate the impact of multipath signals on the respiration signal, we attach an RFID tag on a person's chest and ask another two persons to walk nearby. The received signal phase which is mixed with respiration and multipath signals is shown in Fig. 10a. The ground truth signal of respiration is collected with a chest band and shown in Fig. 10b. The monitored person is asked to breathe normally for 5 respiration cycles. In Fig. 10a, the respiration cycles are messed up with noises caused by multipath signals. In particular, the noises in the green rectangular exhibit similar magnitude as the real respiration peaks. If a low pass filter is applied on Fig. 10a followed by a peak detection scheme, as shown in Fig. 10c, 7 respiration cycles will be detected, and the extra 2 fake respiration cycles could lead to inaccurate respiration rate estimation. Besides, multipath signals would cause wrong apnea detection. If people are moving around the monitored person with the apnea syndrome, multipath signals will incur a similar pattern as respiration, which could misguide that the monitored person is still breathing.

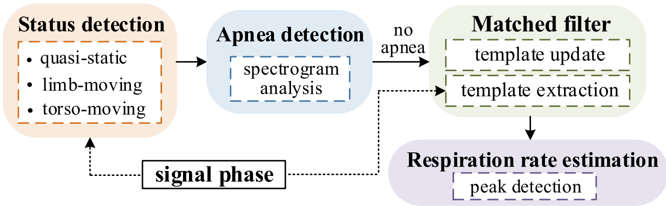

Fig. 11. Overview of the RM-Dynamic system.

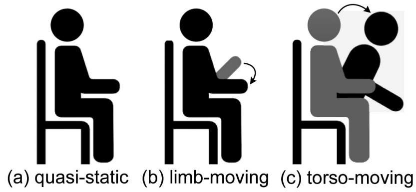

Fig. 12. Three status of the monitored person.

3 Our Approach

In this section, we first give an overview of the RM-Dynamic system. Then, we introduce our proposed methods for eliminating the effect of the multipath signals in dynamic environments for accurate apnea detection and respiration rate estimation.

3.1 Overview

The overview of the RM-Dynamic system is depicted in Fig. 11. The raw signal phase is first collected from the tag on the monitored person's chest and segmented into fix-length windows. Next, status detection is performed to detect whether the monitored person is quasi-static, having small-scale limb movement, or with large-scale torso movement. RM is carried out when large-scale torso movements are not detected. Then, we transform the signal phase into the spectrogram to detect the abnormal pattern of the apnea in the frequency domain. If no apnea is detected, the matched filter is applied on the signal phase to denoise the respiration signal mixed with multipath signals. The matched filter is created using the respiration cycle template generated from our template extraction method. Since different people have various respiration patterns, we pre-collect the signal phase when the monitored person breathes in a static environment to extract a unique template. Besides, we propose a template update method to adapt to the change of the monitored person's respiration pattern along with time. Finally, the filtered signal phase will be processed to estimate the respiration rate by detecting the repetitive peaks.

3.2 Status Detection

Human movement status may significantly impact the RM result. Thus, before performing RM, we first detect the movement status of the monitored person. In our study, we classify the common moving status into three categories, including the quasi-static status (the person only breathes without other movements), limb-moving status (the person has small-scale limb movements), and torso-moving status (the person has large-scale torso movements), as shown in Fig. 12.

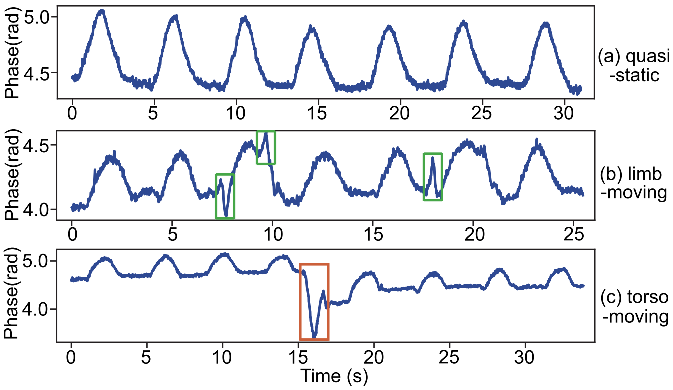

Fig. 13. Signal phase for respiration under different movement status.

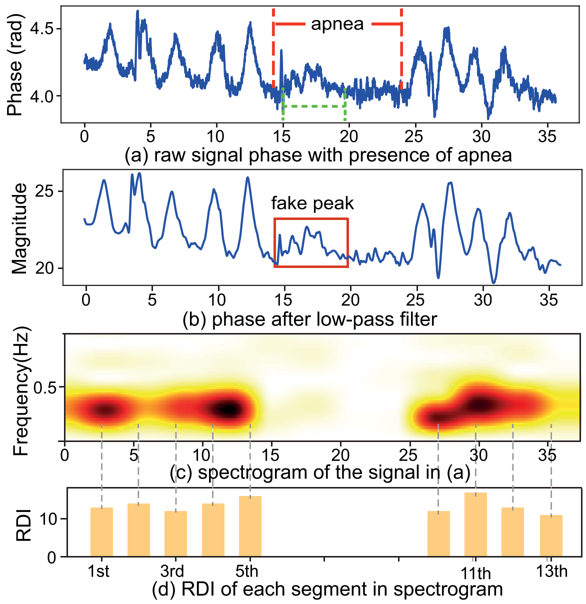

Fig. 14. Raw phase, phase after matched filter, spectrogram, and RDIs for the respiration signal with apnea.

To detect different moving status, we observe the signal phase when a monitored person breathes under the above three status, as shown in Fig. 13. For the quasi-static status, the respiration signal shows a clear periodic pattern. For the limb-moving status, the limb movement causes small jitters in the respiration signal, as the green rectangular depicted in Fig. 13b. These jitters, however, have a limited impact on the respiration signal and can be removed using our designed matched filter. When the monitored person moves the entire torso, the signal phase exhibits more dramatic fluctuations, as highlighted by the red rectangular in Fig. 13c. This is because the human torso may block the LOS path between the tag on the chest and the antenna. Based on these observations, our RM-Dynamic system should automatically detect the movement status and perform RM when the person is in the quasi-static and limb movement status, while stopping RM when large torso movements are detected.[1]

To detect the torso-moving status, we compare the magnitude of the phase changes within a window, which is calculated as the difference ϕ_{diff} between the maximum and minimum phase. If ϕ_{diff} is larger than a pre-defined threshold, the window is regarded as the one under torso-moving status, and vice versa. To obtain the threshold, we first calculate a theoretical value for the maximum phase change ϕ_{r_m} of the respiration signal. The displacement of chest during respiration ranges from $4-12\ mm$ [26]. For the RFID signal with the $925\ MHz$ carrier frequency, ϕ_{r_m} is calculated as $(2d_{r_m}/\lambda)\cdot 2\pi = 0.465\ rad$, where d_{r_m} is set to $12\ mm$. Then, we obtain the empirical standard deviation $\phi_{r_{std}}$ of all the ϕ_{r_m} calculated from the measured respiration signal. Finally, the threshold is determined as the sum of the theoretical ϕ_{r_m} and empirical $\phi_{r_{std}}$.

3.3 Apnea Detection

After status detection, the next step is to detect whether the apnea appears. Recall that multipath signals from moving people could result in fake respiration cycles, which can lead to mis-detection of apnea. For example, the signal phase shown in Fig. 14a is collected from a person who stops breathing from 15 - 24 s with people moving around. The multipath signals result in a respiration-like peak from 15–20 s in the signal phase after the low-pass filter, as shown in the red rectangular of Fig. 14b. Then, the person would be mis-detected as breathing normally after applying the peak detection scheme on the filtered phase.

To differentiate the apnea from multipath signals, we employ the time-frequency pattern of the signal phase. In specific, we extract the spectrogram of the signal phase, from which we can identify the anomaly in the respiration signal with apnea. For instance, the spectrogram of the signal phase in Fig. 14a is extracted and shown in Fig. 14c. The signal spectrogram exhibits a white area in the middle which exactly matches the apnea period, meanwhile clearly showing the dominant frequencies during normal breathing at around $0.3-0.4\ Hz$, which corresponds to the respiration frequency. This indicates that the frequency components of the real respiration signal, although mixed with the multipath signals, still dominant over the respiration frequency range of $0.17-0.5\ Hz$ [25]. In contrast, if the person stops breathing, and only multipath signals are left, the frequency components almost disappear within the respiration frequency range.

Based on this observation, we leverage the disappearance of the dominant frequencies within the respiration frequency range to detect the apnea. We define a respiration-dominance index (RDI) to detect whether the dominant frequency disappears within the respiration frequency range. To measure RDI, we first perform the short-time fourier transformation (STFT) on the signal phase to obtain the spectrogram. In STFT, the signal phase is first divided into fixed-length segments.[2] For each time segment, we measure the mean of all the frequency-domain amplitudes in the spectrogram as a noise threshold. Then, the RDI is calculated by counting the number of frequencies, whose amplitude exceeds the noise threshold within the respiration frequency range. RDI characterizes the dominance of the

1. We note that torso-moving status, e.g., posture change during sleep, does not appear frequently. The monitor person is mostly in a quasi-static status or with a few limb movements.

2. In our implementation of STFT, the length of the segment is set to 512 sampling points, and the size of FFT is 2,048 after zero-padding.

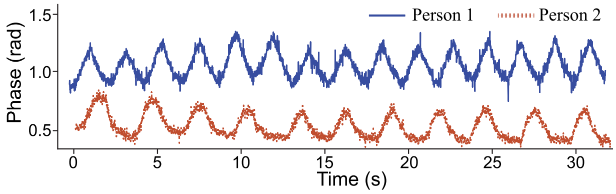

Fig. 15. Phase values of two persons' respiration activity.

respiration components over all the frequency components in each segment of the signal phase. The RDI of multipath signals during the apnea period is much lower than that of the respiration cycles mixed with multipath signals. In Fig. 14d, we show the RDIs for all the segments of the spectrogram in Fig. 14c. RDIs during the apnea period all decrease to 0 while the RDIs for the respiration cycles all exceed 10. To detect the decrease in RDIs for apnea detection, we calculate the mean RDI of the person's pre-collected respiration signal in the static environment, and half of the mean RDI is set as the reference RDI. If the length of consecutive RDIs whose values are lower than the reference RDI exceeds $5\ s$, the apnea is detected, and the corresponding phase window will not be used to perform respiration rate estimation. The length of $5\ s$ is chosen because it is the longest duration of normal respiration cycles [25].

3.4 Matched Filter

After apnea detection, the signal phase without apnea is used to estimate the respiration rate. Recall that the real respiration cycles are distorted by high-frequency noises and fake respiration cycles, which cannot be simply eliminated by the low-pass filter. To tackle this issue, we leverage the difference between the respiration pattern and multipath signals. In specific, due to the intrinsic features of the human respiration pattern, the respiration signal phase shows a periodic and sinusoidal pattern. In contrast, multipath signals are random and irregular, which involve both low and high-frequency noises combined in various ways. This inspires us to employ the matched filter to detect the target signal out of noises. The matched filter is an optimal linear filter, created from a target signal template, to detect the target signal by maximizing its signal-to-noise ratio (SNR) from the unknown signal mixed with noises [27]. For RM, we extract a single respiration cycle as the template for creating the matched filter and apply the matched filter on the received signal phase to denoise it. The output of the matched filter will peak at where the target signal appears. Finally, we can detect the peaks in the filtered phase and estimate the respiration rate.

3.4.1 Template Extraction

To design the matched filter, the respiration cycle template should be carefully selected due to the following reasons. First, the shape of the template can affect the performance of the matched filter. Only when the template has the same shape as the target signal can we achieve the optimal SNR. If the shape of the template is not consistent, the SNR of the matched filter output will vary accordingly. Second, respiration patterns are unique and diverse among different people [20]. For example, the signal phase of two persons' respiration in Fig. 15 shows that their respiration cycles have different shapes. This means that the respiration cycle template should be typical for each monitored person to achieve higher SNR of the filtered phase. We will discuss the effect of using the person's own template and other persons' templates on the SNR in Section 4.

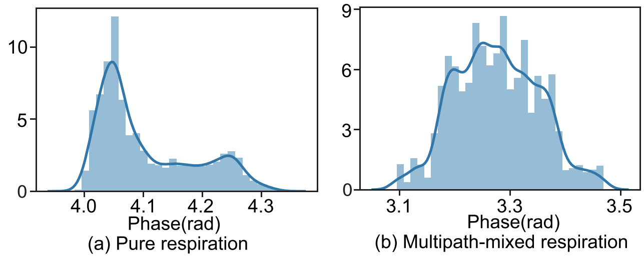

Fig. 16. Distributions of the signal phase for (a) the pure respiration signal and (b) respiration signal mixed with the multipath signals.

To extract the respiration cycle template, we first pre-collect the signal phase of pure respiration for the monitored person in a static environment. The monitored person normally breathes for $1-2$ minutes during which the signal phase is collected. Noth that the template collection is a one-time step, which would not bring too much inconvenience to users. Then, we extract the template from the pure respiration signal by using a cycle-averaging method introduced as follows. First, we smooth the respiration signal phase with a median filter. Then, we detect the local minimums, which are the starting points of respiration cycles, to segment the signal phase into individual cycles. To detect the local minimums, peak detection is performed on the negative of the signal phase. Next, for each respiration cycle, we calculate its similarity with all the other respiration cycles using the euclidean distance. The respiration cycle with the highest similarity is selected as the template candidate. Finally, the template candidate is scaled according to the average width and height of all the respiration cycles as the respiration cycle template $r_t(n)$.

3.4.2 Template Update

In practice, people's respiration patterns may change along with time. Respiration rate can increase or decrease under different scenarios. For instance, the respiration rate could increase after doing exercise. Furthermore, many diseases, e.g., tachypnea and bradypnea, are related to the increasing and decreasing of respiration rate. As such, the template for the matched filter should be timely updated to adapt to the change of respiration pattern.

herefore, we propose a template update method during RM. We first set a period for updating the template, e.g., $3\ min$, considering that the respiration pattern is highly possible to remain stable in a short period. Then, for each update period, a certain time window of the signal phase, which is only affected by the respiration activity without the interference from multipath signals, is applied to update the template. To achieve this, we leverage the difference of the phase distributions between the pure respiration signal and the respiration signal mixed with the multipath signals. The pure respiration signal is a sinusoidal wave, which has a non-gaussian distribution, as shown in Fig. 16a. While,

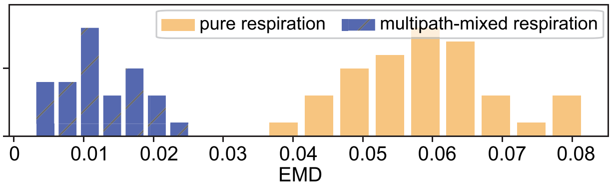

Fig. 17. EMD between the gaussian distribution and the distributions of the pure respiration signal and multipath-mixed respiration signal.

due to the random noises incurred by the multipath signals, the distribution of the multipath-mixed respiration signal is more likely to be gaussian, as depicted in Fig. 16b. Based on these observations, we calculate the distance between the phase distribution and a comparison gaussian distribution. The earth mover's distance (EMD) is employed to measure the distribution distance. A smaller EMD indicates a larger similarity. The mean and standard deviation of the comparison gaussian distribution are set to be those obtained from the measured signal phase. We collect 40 traces of phase for the monitored person breathing normally in a static environment and with people moving nearby, respectively. Their EMD results with the corresponding gaussian distribution are shown in Fig. 17. For the pure respiration signal, the distance is much larger than that of the multipath-mixed respiration signal. Hence, we select the phase window whose EMD is the largest among all the windows so that it mainly involves the pure respiration signal. Then, the cycle-averaging method is applied on the selected window to update the template $r_t(n)$.

3.4.3 Matched Filter Creation

With the extracted template $r_t(n)$, the impulse response of the matched filter $h(k)$ is obtained as $h(k) = r_t(N-k-1)$, where N is the length of $r_t(n)$. In Fig. 18, we show the output signal phase after applying the matched filter on the raw signal phase in the upper figures of Figs. 18a and 18b, respectively. In the first figure of Fig. 18a, the multipath signals from surrounding movements bring fake respiration cycles in the raw signal phase. When using the low-pass filter, these fake cycles still remain in the signal phase. In contrast, applying the matched filter can remove the fake cycles meanwhile accurately detecting the real cycles, which match the ground truth in Fig. 10b. Similarly, by applying the matched filter, the fake respiration peak caused by the limb movement in Fig. 18b, is successfully removed, which, however, cannot be fulfilled by the low-pass filter.

3.5 Respiration Rate Estimation

Intuitively, we can apply fast fourier transformation (FFT) to measure the respiration rate. However, the resolution of FFT is restricted by the length of the time window [12]. For instance, if respiration rate is measured every 20 s, the resolution in the frequency domain is 0.05 Hz, which results in 3 bpm resolution in the time domain. Thus, to accurately estimate the respiration rate, we use peak detection to avoid the low-resolution problem of FFT.

The peak detection method estimates the respiration rate based on the detected peaks, which is suitable for real-time respiration monitoring. However, the peak detection approach could suffer from tiny fluctuations, which can be misdetected as peaks, in the filtered phase. Previous methods set thresholds to discard the wrong peaks which are too low or too closed to each other [7]. However, in the RM scenario, the magnitude of the signal phase will change along with time. A fixed threshold may be improper and could incur missing or wrong peaks. Therefore, to adapt to different scales automatically, we employ the automatic multiscale peak detection (AMPD) [28] algorithm. AMPD frees us from choosing fixed thresholds to detect the real peaks with the help of the multi-scale technique. The detected peaks of the signals in Fig. 18 after applying AMPD are shown with red crosses. Then, the respiration rate is estimated as follows.

$$rate = 60/\frac{1}{n}\sum_{i}^{n-1}(p_{i+1}-p_i), \tag{6}$$

where p_i is the timestamp of the detected peak, and n is the total number of peaks. The calculated respiration rate is in the unit of breath per minute (bpm).

4 Evaluation

In this section, we introduce the experimental setup, evaluation metrics, and experimental results in terms of different factors for apnea detection and respiration rate estimation.

4.1 Experimental Setup

We implemented the RM-Dynamic system using commercial off-the-shelf RFID devices. The ImpinJ Speedway R420 reader is connected with a Laird E9208 antenna to transmit the RFID signal and interrogate the RFID tag. The reader

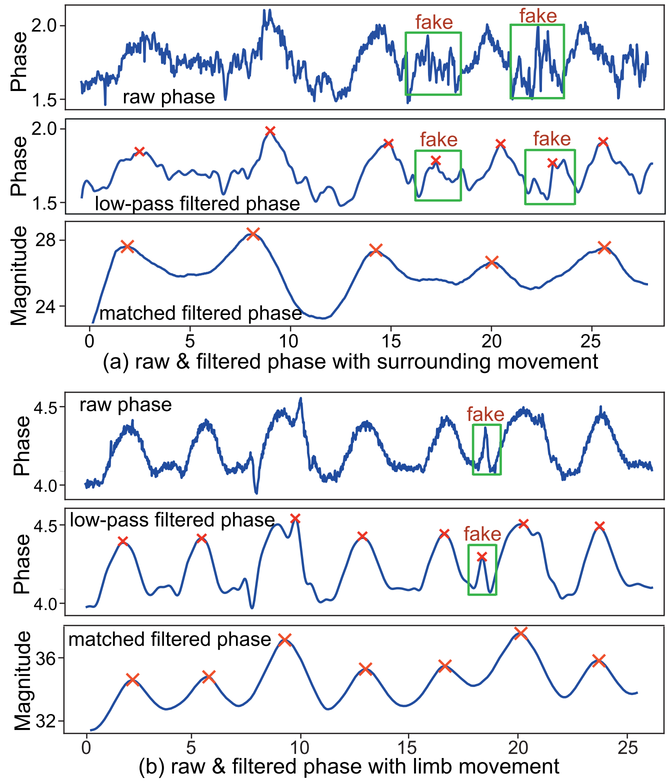

Fig. 18. Raw and filtered phase mixed with the multipath signals from (a) the ambient movement of surrounding people and (b) the limb movement of the monitored person.

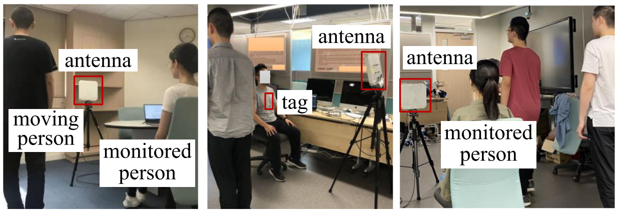

Fig. 19. Experimental settings in different environments.

works in the $920-925$ MHz frequency band, and the reader mode is set to MaxThroughput. The reader is connected to a Dell Inspiron 7460 laptop with i7-7500U CPU and 8 GB RAM. The RFID signal phase is processed using Python 3.0.

We conducted experiments in three different environments with different layouts, as shown in Fig. 19. The antenna is placed $1-2$ m away from the monitored person. The tag is attached on the person's chest. We invite 12 volunteers, including 3 females (height: $165-170$ cm, chest width: $27-32$ cm) and 9 males (height: $172-180$ cm, chest width: $33-40$ cm), to act as the monitored person and surrounding people in turn. We do not assign specific routes for volunteers to move so that they can walk freely nearby the monitored person. We ask the monitored person to normally breathe for 2 min to extract the respiration template. Then, the signal phase is segmented into 20 s-windows to estimate the respiration state. The ground truth of the respiration signals is collected via a chest band equipped with a 3-axis accelerometer.

4.2 Evaluation Metrics

We use the following metrics to evaluate the performance of our system. First, for apnea detection, the percentage of the missing apnea (MA) and false apnea (FA) over all the apnea cases are defined as below.

$$MA = \frac{\#missing\ apnea}{\#real\ apnea},\ FA = \frac{\#false\ apnea}{\#no\ apnea}. \tag{7}$$

Second, to evaluate the accuracy of respiration rate estimation, we use the mean absolute error (MAE) as below.

$$MAE = \frac{1}{n}\sum_{i=1}^{n}|r_i - r_i^{'}|, \tag{8}$$

where r_i and $r_i^{'}$ are the estimated and real respiration rate, respectively. n is the number of time windows.

4.3 Evaluation Results

In this section, we show the experimental results on apnea detection and respiration rate estimation.

4.3.1 *Performance of Status Detection*

First, we evaluate the accuracy of our method for status detection, which aims to differentiate the large-scale torso movement from the quasi-static and small-scale limb movement of the monitored person. The respiration state estimation, including apnea detection and respiration rate estimation, is performed when the monitored person is in the quasi-static status or with small-scale limb movement. In this evaluation, we ask all the volunteers to breathe normally in the quasi-static status, breathe with little limb movement (e.g., shake the hand), breathe with torso movement (e.g., turn around the body), and collect the corresponding signal phase, respectively. The status detection results are shown in Table 1. The accuracy of detecting the quasi-static & limb-moving status and the torso-moving status both exceed 95%. Such a status detection result guarantees that RM can be accurately performed.

TABLE 1
Accuracy of Status Detection

	quasi-static & limb-moving	torso-moving
Accuracy	95.7%	97.1%

TABLE 2
Comparison of RDI-Based and Peak-Threshold Based Methods for Apnea Detection

	RDI (our method)	peak-threshold
MA	3.75%	12.65%
FA	4.15%	15.8%

4.3.2 *Effect of RDI for Apnea Detection*

In this evaluation, we compare the performance of our RDI-based approach with the existing peak-threshold approach [9] to demonstrate the effectiveness of our approach on apnea detection in dynamic environments. The previous approach sets a fixed threshold for detecting peaks in the respiration signal. If there is no peak for a certain time, the apnea is detected. We set the same threshold in [9], which is the median of the signal phase in a time window, and compare its result with our RDI-based method. Table 2 shows that our approach outperforms the peak-threshold approach with an approximate 10% reduction of MA and FA. This is because the fake peaks caused by the multipath signals from moving people are wrongly regarded as breathing cycles in the peak-threshold approach. However, our proposed RDI-based approach can accurately differentiate the real respiration signal from the multipath signals during the apnea period.

4.3.3 *Effect of Matched Filter for Respiration Rate Estimation*

To show the effectiveness of the matched filter on respiration rate estimation, we first compare the MAE between the real and estimated respiration rates with and without applying the matched filter on the signal phase. For methods without the matched filter, we use the low-pass filter and median filter to denoise the signal phase. Then, AMPD is applied to count the respiration cycles. As shown in Fig. 20a, the average MAE using the matched filter is 0.51 bpm. While the MAEs using the low-pass and median filters are 2.94 bpm and 3.08 bpm, respectively, which are 5 times larger than that of using the matched filter. This indicates that the matched filter can help to promote the accuracy of respiration rate estimation.

Next, we investigate the effectiveness of the template extraction and update methods with two experiments. The first experiment is to show how different persons' templates

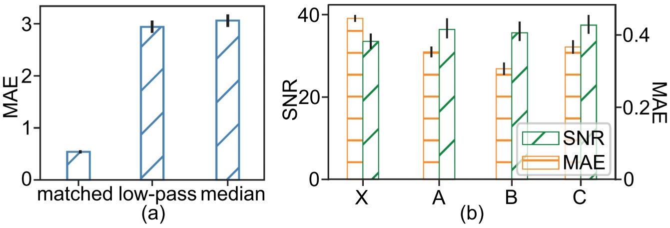

Fig. 20. Effect of matched filter: (a) MAE for respiration rate estimation with matched filter, low-pass filter, and median filter (b) SNR and MAE of using different respiration templates to make matched filter.

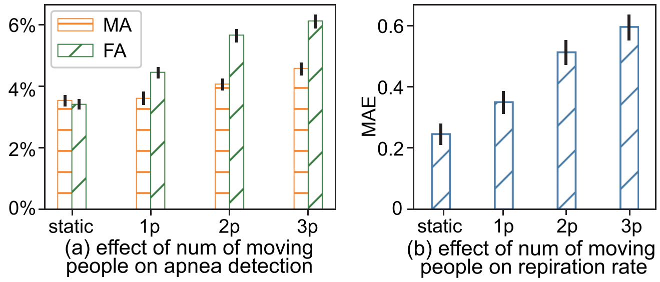

Fig. 21. Effect of the number of moving people on (a) apnea detection, (b) respiration rate estimation.

could affect the RM performance. We select one volunteer (X) and extract the template from X's respiration signal phase in a static environment. Then, X's template is used to create a matched filter to denoise the respiration signal phase when people move around X. Then, we extract another three templates from three volunteers (A, B, and C) and create three matched filters, respectively. Finally, we apply the three matched filters to denoise X's respiration signal phase. The MAEs of using the matched filters created from different persons' templates are shown in Fig. 20b. In addition to the MAE, SNR is also reported to show the ability of the matched filter for denoising the signal. The SNR when using the matched filter created from X's own template is higher than using other persons' templates. Meanwhile, using X's own template also achieves the lowest MAE, indicating the importance of extracting the personalized template for each user and the effectiveness of our template extraction method.

The second experiment is to show the performance of the template update method when the monitored person changes the respiration pattern. We let X breathe normally for $5\ min$ with other people moving nearby and collect the respiration signal phase. Then, X is asked to do pedaling for $15\ min$. After pedaling, the respiration rate of X greatly increases, and we continue to collect X's signal phase for $10\ min$. Then, we estimate the respiration rate before and after pedaling using a fixed template and the updated templates of X, respectively. The template update period is set as $2\ min$. The MAE of using the update templates is $0.11\ bpm$ lower than the fixed template, showing the effectiveness of the template update method.

4.3.4 Effect of the Number of Moving People on Apnea Detection and Respiration Rate Estimation

In this evaluation, we evaluate the system performance in both static and dynamic environments with different numbers of moving people, i.e., 0 (static), 1 (1p), 2 (2p), and 3 (3p) persons moving around. The distance between the person and antenna is set as $1.5\ m$. First, we evaluate the apnea detection performance. Volunteers who act as the monitored person are asked to simulate the apnea by holding their breath for $5{-}10\ s$. The results of MA and FA are shown in Fig. 21a. Generally, MA and FA grow slightly with the increasing number of moving people, while they are both below 6% for all cases. The average MA and FA with 1-3 moving persons are only 2-3% higher than those in the static environment. This indicates that our approach can enhance the robustness of apnea detection in dynamic environments with multiple surrounding persons.

We further show the MAE of respiration rate estimation for different numbers of moving people in Fig. 21b. The average MAE raises from $0.2\ bpm$ to $0.6\ bpm$ with more number of moving people. This is mainly because more moving people could result in more multipath signals. We also compare the accuracy of respiration rate estimation of our system with existing systems in Table 3. Our system has a similar range of MAE compared with existing works. Furthermore, [12], [14] are only designed for RM in static environments, while our system can also work in dynamic environments.

TABLE 3
Comparison of Respiration Rate Estimation With Existing Work

	[12]	[14]	our approach
MAE	0.5-1 bpm	0.3-0.5 bpm	0.3-0.6 bpm
Scenario	static	static	dynamic

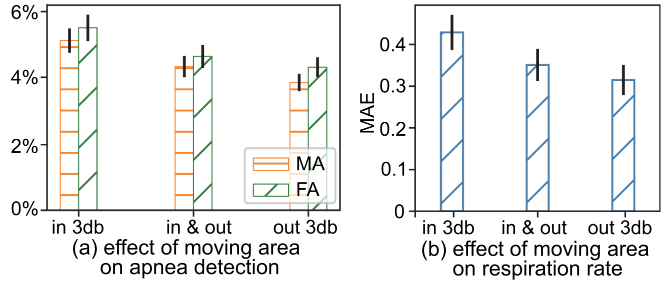

Fig. 22. Effect of the moving area of surrounding people for (a) apnea detection, (b) respiration rate estimation.

4.3.5 Effect of the Moving Area of Surrounding People on Apnea Detection and Respiration Rate Estimation

As mentioned in Section 2.2.1, the moving area could affect the signal phase. Hence, we ask a volunteer to move inside, outside, and randomly inside or outside the $3\ dB$-area to test the system performance, respectively. First, we show the results of apnea detection in different areas in Fig. 22a. MA and FA when the ambient person moves outside the $3\ dB$-area are around 4%, which are smaller than the MA and FA of moving inside the $3\ dB$-area. For randomly moving in and out of the $3\ dB$-area, MA and FA are slightly larger than that of moving outside the $3\ dB$-area.

The MAEs for respiration rate estimation of different moving areas are shown in Fig. 22b. When the person

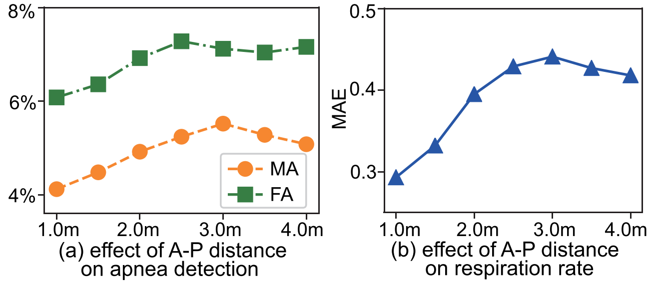

Fig. 23. Effect of the distance between the monitored person and antenna for (a) apnea detection, (b) respiration rate estimation.

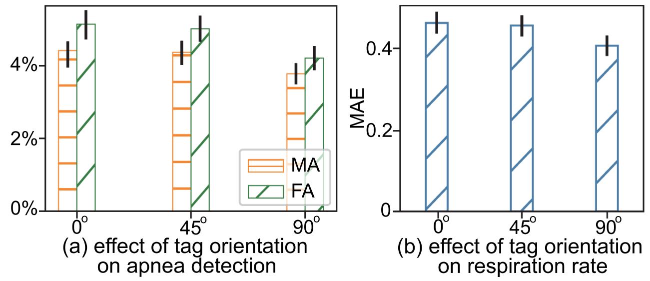

Fig. 24. Effect of the tag orientation for (a) apnea detection, (b) respiration rate estimation.

moves inside the 3 dB-area, the MAE is around 0.45 bpm, which is 0.15 bpm higher than moving outside the 3 dB-area in average. The results show that we can still achieve relatively high accuracy when the moving person is inside the 3 dB-area of the antenna.

4.3.6 Effect of Distance Between Antenna and Monitored Person on Apnea Detection and Respiration Rate Estimation

In this evaluation, we investigate the effect of the distance between the antenna (A) and the monitored person (P) on the system performance. A longer distance between A and P means a longer traveling distance of the RFID signal, resulting in a more attenuated backscattered signal. Besides, the longer the distance between A and P, the larger the 3 dB-area is. As such, people may easily move into the 3 dB-area. In our experiment, we first change the $A-P$ distance from 1 m to 4 m with an interval of 0.5 m to test how the distance affects the accuracy of apnea detection. Then, we ask one volunteer to move nearby the monitored person. The results of apnea detection under different distances are shown in Fig. 23a. Both the MA and FA increase along with the increasing distance between A and P. MA and FA slightly drop when the distance exceeds 2.5–3 m because the power of the multipath signals reflected by the moving person would decrease with a longer $A-P$ distance. The error difference of apnea detection with different $A-P$ distances is around 1.5%.

The MAEs of respiration rate estimation for different distances are shown in Fig. 23b. The MAE gradually goes up when the distance increases from 1 m to 3 m. This is because the 3 dB-area becomes larger to allow the person to move inside, and multipath signals bring a larger effect on the signal phase. While, when the distance is larger than 3 m, the MAE slightly drops because the multipath signals become weak with a longer traveling distance. Furthermore, a longer distance between A and P also leads to weaker respiration LOS signals.

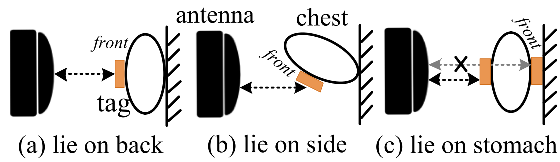

Fig. 25. Three kinds of common sleeping postures, including (a) lie on the back, (b) lie on the side, (c) lie on the stomach.

TABLE 4
Apnea Detection and Respiration Rate Estimation Results Under Different Sleeping Postures

Posture	Apnea Detection		Respiration rate estimation (MAE)
	MA	FA	
Lie on back	3.9%	4.5%	0.38 bpm
Lie on side	5.4%	5.8%	0.54 bpm
Lie on stomach	front tag: / back tag: 7.8%	front tag: / back tag: 8.6%	front tag: / back tag: 0.62 bpm

4.3.7 Effect of Tag Orientation on Apnea Detection and Respiration Rate Estimation

When being attached on the chest, the tag can be placed with different orientations. Different orientations of the tag could result in different initial signal phases of the backscattered signal [29], which affects the system performance. In our experiment, we choose 3 orientations, including 0°, 45°, and 90° of the tag to the gravity direction. The results for apnea detection with different orientations are given in Fig. 24a. The MA and FA under all tag orientations are lower than 5% for apnea detection, and the MAE of respiration rate estimation is only around 0.4 bpm as shown in Fig. 24b. This is because we make sure the LOS path exists throughout the experiment and we use the relative phase change to measure the chest displacement. In addition, we use a circularly polarized antenna which covers all tag orientations and can receive the consistent backscattered signal under different tag orientations.

4.3.8 Effect of Different Postures

In this experiment, we evaluate our method for apnea detection and respiration rate monitoring for different sleeping postures. We mainly consider three common postures, i.e., lying on the back, lying on the side, and lying on the stomach, as shown in Fig. 25. We ask one volunteer to lie under three different postures and ask another volunteer to walk nearby. The results are shown in Table 4. The accuracy of both apnea detection and respiration rate estimation for the posture of lying on the side is lower than those of lying on the back. This is because when the user lies on the side, the chest displacement brings a smaller change of the signal phase. When the user lies on the stomach, since the signal of the front tag is fully blocked by the body, the reader cannot receive the backscattered signal. However, we notice that the human

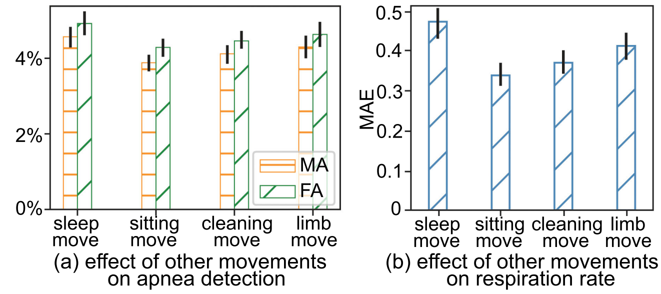

Fig. 26. Effect of the other movements, including sleeping posture changes, sitting movements, cleaning room, and limb movements of the monitored person for (a) apnea detection, (b) respiration rate estimation.

back still expands and contracts slightly during respiration. Thus, we attach another tag on the back for RM. As shown in Table 4, the MA and FA of apnea detection are still below 10%, and the MAE for respiration rate is still below $0.7\ bpm$, which reveals the validity of our proposed system.

4.3.9 Performance of Other Movements

Apart from the walking movement, other movements could also appear around the monitored person in daily RM scenarios. In this experiment, we evaluate the system performance for another four common movements. First, for the couple in sleep, the movement of one person changing the sleeping posture can bring multipath signals to the other person being monitored. Thus, we ask two volunteers to lie down. One of them is the monitored person and another volunteer act as the surrounding person who is around $30\ cm$ away from the monitored person and is allowed to randomly change sleeping postures. Second, for a person sitting beside the monitored person, the person's movements like stretching arms or turning around also incur multipath signals to the monitored person. Therefore, we ask one volunteer to sit $50\ cm$ away from the monitored person and move his/her arm and body. Third, in home environments, the housekeeper may move nearby the monitored person. Finally, the monitored person could move limbs during RM. We conduct experiments under the above four scenarios to detect the apnea and measure the respiration rate.

The results are shown in Fig. 26. The MA and FA of apnea detection are all below 5% for different movements. This is because our designed matched filter can remove the effect of the surrounding person's movement and small-scale limb movement from the monitored person. The sitting movements have the lowest MA and FA mainly because they introduce a relatively smaller scale of movements. Meanwhile, the sleeping posture changes and limb movements have a relatively larger effect on apnea detection. This may due to the reason that these movements are more close to the monitored person, i.e., inside the $3\ dB$-area, so that more significant multipath signals are incurred. The MAE of respiration rate estimation shows similar results, with the MAE of less than $0.5\ bpm$.

5 Related Work

Our work is related to RF-based RM and the multipath effect of RF signals. Therefore, in this section, we introduce existing works for RF-based RM and solutions in dealing with the multipath effect.

5.1 RF-Based RM

Existing works employ RF technologies, e.g., WiFi, Radar, and RFID, for RM since these technologies enable a convenient and non-intrusive method for RM. WiFi has been popularly used for RM due to its low-cost and pervasive features [5], [6], [7], [9], [30], [31], [32]. The Fresnel zone model is introduced to explain the principle and theory of using the WiFi signal for RM [6]. This model jointly considers the effect of the user's location and the WiFi sensing range to achieve optimal RM performance. Based on this model, FarSense further employs the ratio of WiFi channel state information to greatly increases the sensing range of WiFi signal [30]. In addition to RM, heartbeat estimation can be achieved using the WiFi signal as well [7]. However, WiFi technology suffers from narrow bandwidth, which is difficult to realize simultaneous RM for multiple users. Although multi-user RM has been investigated using WiFi technology [9], [31], [33], they fail to match the respiration pattern to each person because the narrow bandwidth of WiFi cannot localize multiple users accurately. However, the mapping among the multiple users and respiration patterns is critical so that users can know which person has respiratory problems. To overcome this limitation, UWB and FMCW radar are employed to monitor the respiration since these devices can provide wider bandwidth [10], [11], [34]. However, such specialized devices are expensive and difficult for public use and large-scale deployment.

In recent years, RFID is widely used for RM due to the lightweight and cost-effective RFID tags [12], [13], [14], [15], [17], [35], [36]. TagBreathe uses commodity RFID readers and enables multi-user RM by attaching RFID tags on multiple users and separately extracting the signal phase from each tag on the basis of the tag ID [12]. RFID signal can be used for RM under different applications, for instance, RM is realized when people are doing during exercise [15] and driving in a car [35]. Apart from RM, the RFID signal can detect respiration and heartbeat simultaneously [16]. However, existing approaches either work in a static environment or when the monitored person is moving, e.g., walking or running. Our work differs from previous works that we implement RM in the dynamic environment, where other people could move nearby the monitored person. Our proposed RM-Dynamic system aims to fill this gap for RFID-based RM.

5.2 Multipath Effect of RF Signals on RM

The multipath effect is a propagation phenomenon for RF signals. This phenomenon is common in practice because there are many reflectors in our environment that can reflect RF signals [37]. Multipath signals reflected by non-target objects can bring noises for sensing the target object's behavior. Different approaches have been proposed to deal with the multipath effect [38], [39], [40], [41]. WiTrack employs FMCW radar to extract the time of flight of each signal path, so that the LOS signal of the target person, which has the shortest path, can be separated from multipath signals [39]. RespiRadio revises the WiFi 802.11

protocol to widen the bandwidth of the WiFi signal and employs the channel impulse response to separate the target's signal path from other multipath signals [38]. Instead of using the expensive FMCW radar or modifying the WiFi protocol, we provide a lightweight approach to remove the multipath effect with RFID technology. In our work, based on our detailed investigation on how multipath signals affect the respiration signal, we effectively remove the noises caused by multipath signals for accurate RM without introducing extra hardware or any modification of the standard communication protocol.

6 Discussion

In this section, we discuss some practical issues in using our system. First, for sleep apnea detection, the current system can only detect the central apnea, which is caused by a failure of the brain to activate the muscles of breathing, so that there is no chest movement. But for the obstructive apnea, in which the chest muscle still moves but the airway is blocked, we cannot detect it. In fact, existing RF-based RM systems all fail to do so, because the principle of using RF signals for RM is to detect signal change incurred by the chest movement during breathing.

Second, in the current system, we practically assume that surrounding people would mainly move in the vicinity of the monitored person without going across the LOS path between the monitored person and antenna. This means that RM-Dynamic is not designed to remove the effect from the surrounding people if they move to block the LOS path. While in practice, we can change the deployment of the RFID antenna to avoid other people blocking the LOS path.

7 Conclusion

In this work, we aim to achieve robust RFID-based RM in dynamic environments. Previous systems have realized RM in the static environment. While in dynamic environments, the moving people bring multipath signals which distort the respiration pattern in the RFID signal phase. Therefore, we propose to enhance the robustness of RFID-based RM in dynamic environments. To identify the apnea out of the multipath signals which could mimic the pattern of breathing cycles, we draw on the dominance of respiration components in the frequency domain to avoid the missing detection of apnea. For respiration rate estimation, the effect of the multipath signals is eliminated by employing the matched filter to detect the desired respiration cycles from the noisy signal phase. The respiration rate is then obtained by counting the peaks in the filtered phase. The evaluation results show that our approach can promote the accuracy of respiration monitoring in dynamic environments.

Acknowledgments

The work was supported by HK RGC Collaborative Research Fund No. C5018-20G, HK RGC General Research Fund No. PolyU 15220020, the National Nature Science Foundation of China under Grant 62102139, and the Fundamental Research Funds for the Central Universities under Grant 531118010612.

References

[1] "Sleep apnea," Accessed: Sep. 1, 2019. [Online]. Available: https://www.nhlbi.nih.gov/health-topics/sleep-apnea,

[2] "The importance of respiratory rate monitoring," Accessed: Oct. 1, 2019. [Online]. Available: https://doi.org/10.12968/bjon.2019.28.8.504

[3] "Chronic respiratory diseases," Accessed: Sep. 1, 2019. [Online]. Available: https://www.who.int/health-topics/chronic-respiratory-diseases

[4] M. Elliott, "Why is respiratory rate the neglected vital sign? A narrative review," *Int. Arch. Nurs. Health Care*, vol. 2, no. 3, 2016, Art. no. 050.

[5] X. Liu, J. Cao, S. Tang, and J. Wen, "Wi-sleep: Contactless sleep monitoring via wifi signals," in *Proc. IEEE RTSS*, 2014, pp. 346–355.

[6] H. Wang *et al.*, "Human respiration detection with commodity wifi devices: Do user location and body orientation matter?" in *Proc. ACM Ubicomp*, 2016, pp. 25–36.

[7] J. Liu, Y. Wang, Y. Chen, J. Yang, X. Chen, and J. Cheng, "Tracking vital signs during sleep leveraging off-the-shelf wifi," in *Proc. ACM MobiHoc*, 2015, pp. 267–276.

[8] T. Rahman *et al.*, "Dopplesleep: A contactless unobtrusive sleep sensing system using short-range doppler radar," in *Proc. ACM Ubicomp*, 2015, pp. 39–50.

[9] X. Wang, C. Yang, and S. Mao, "Phasebeat: Exploiting CSI phase data for vital sign monitoring with commodity WiFi devices," in *Proc. IEEE ICDCS*, 2017, pp. 1230–1239.

[10] F. Adib, H. Mao, Z. Kabelac, D. Katabi, and R. C. Miller, "Smart homes that monitor breathing and heart rate," in *Proc. ACM CHI*, 2015, pp. 837–846.

[11] S. Yue, H. He, H. Wang, H. Rahul, and D. Katabi, "Extracting multi-person respiration from entangled rf signals," in *Proc. ACM Ubicomp*, 2018, pp. 1–22.

[12] Y. Wang and Y. Zheng, "Tagbreathe: Monitor breathing with commodity RFID systems," *IEEE Trans. Mobile Comput.*, vol. 19, no. 4, pp. 969–981, Apr. 2019.

[13] C. Yang, X. Wang, and S. Mao, "Autotag: Recurrent variational autoencoder for unsupervised apnea detection with RFID tags," in *Proc. IEEE GLOBECOM*, 2018, pp. 1–7.

[14] R. Zhao, D. Wang, Q. Zhang, H. Chen, and A. Huang, "CRH: A contactless respiration and heartbeat monitoring system with cots RFID tags," in *Proc. IEEE SECON*, 2018, pp. 1–9.

[15] Y. Yang, J. Cao, and X. Liu, "Er-rhythm: Coupling exercise and respiration rhythm using lightweight cots RFID," in *Proc. ACM Ubicomp*, 2019, pp. 1–24.

[16] C. Wang, L. Xie, W. Wang, Y. Chen, Y. Bu, and S. Lu, "RF-ECG: Heart rate variability assessment based on cots rfid tag array," in *Proc. ACM Ubicomp*, 2018, pp. 1–26.

[17] L. Chen *et al.*, "Lungtrack: Towards contactless and zero dead-zone respiration monitoring with commodity rfids," *Proc. ACM Interactive, Mobile, Wearable Ubiquitous Technol.*, vol. 3, no. 3, pp. 1–22, 2019.

[18] Y. Wang and Y. Zheng, "Modeling RFID signal reflection for contact-free activity recognition," in *Proc. ACM Ubicomp*, 2018, pp. 1–22.

[19] X. Fan, W. Gong, and J. Liu, "Tagfree activity identification with RFIDs," in *Proc. ACM Ubicomp*, 2018, pp. 1–23.

[20] G. Benchetrit, "Breathing pattern in humans: Diversity and individuality," *Respiration Physiol.*, vol. 122, no. 2–3, pp. 123–129, 2000.

[21] P. V. Nikitin, R. Martinez, S. Ramamurthy, H. Leland, G. Spiess, and K. Rao, "Phase based spatial identification of UHF RFID tags," in *Proc. IEEE RFID*, 2010, pp. 102–109.

[22] X. Lai, Z. Cai, Z. Xie, and H. Zhu, "A novel displacement and tilt detection method using passive UHF RFID technology," *Sensors*, vol. 18, no. 5, 2018, Art. no. 1644.

[23] "Rfid antennas," Accessed: Sep. 1, 2019. [Online]. Available: https://media.digikey.com/pdf/Data-Sheets/Laird-Technologies/RFID-Antennas.pdf

[24] T. Ji and A. Pachi, "Frequency and velocity of people walking," *Structural Eng.*, vol. 84, no. 3, pp. 36–40, 2005.

[25] "Respiration rate," Accessed: Sep. 1, 2019. [Online]. Available: https://en.wikipedia.org/wiki/Respiratory-rate

[26] G. Shafiq and K. C. Veluvolu, "Surface chest motion decomposition for cardiovascular monitoring," *Scientific Rep.*, vol. 4, 2014, Art. no. 5093.

[27] R. G. Lyons, *Understanding Digital Signal Processing, 3/E*. Chennai, India: Pearson Education India, 2004.

[28] F. Scholkmann, J. Boss, and M. Wolf, "An efficient algorithm for automatic peak detection in noisy periodic and quasi-periodic signals," *Algorithms*, vol. 5, no. 4, pp. 588–603, 2012.

[29] Y. Bu *et al*. "RF-dial: Rigid motion tracking and touch gesture detection for interaction via RFID tags," *IEEE Trans. Mobile Comput.*, to be published, doi: 10.1109/TMC.2020.3017721.

[30] Y. Zeng, D. Wu, J. Xiong, E. Yi, R. Gao, and D. Zhang, "Farsense: Pushing the range limit of wifi-based respiration sensing with CSI ratio of two antennas," *Proc. ACM Interactive, Mobile, Wearable Ubiquitous Technol.*, vol. 3, no. 3, pp. 1–26, 2019.

[31] Y. Zeng, D. Wu, J. Xiong, J. Liu, Z. Liu, and D. Zhang, "Multisense: Enabling multi-person respiration sensing with commodity WiFi," in *Proc. ACM on Interact., Mobile, Wearable Ubiquitous Technol.*, 2020, pp. 47–56.

[32] D. Wu, D. Zhang, C. Xu, H. Wang, and X. Li, "Device-free WiFi human sensing: From pattern-based to model-based approaches," *IEEE Commun. Mag.*, vol. 55, no. 10, pp. 91–97, Oct. 2017.

[33] X. Wang, C. Yang, and S. Mao, "Tensorbeat: Tensor decomposition for monitoring multiperson breathing beats with commodity WiFi," *ACM Trans. Intell. Syst. Technol.*, vol. 9, no. 1, pp. 1–27, 2017.

[34] Y. Yang, J. Cao, X. Liu, and X. Liu, "Multi-breath: Separate respiration monitoring for multiple persons with UWB radar," in *Proc. IEEE COMPSAC*, 2019, pp. 840–849.

[35] C. Yang, X. Wang, and S. Mao, "Respiration monitoring with RFID in driving environments," *IEEE J. Selected Areas Commun.*, vol. 39, no. 2, pp. 500–512, Feb. 2021.

[36] S. Zhang, X. Liu, Y. Liu, B. Ding, S. Guo, and J. Wang, "Accurate respiration monitoring for mobile users with commercial RFID devices," *IEEE J. Selected Areas Commun.*, vol. 39, no. 2, pp. 513–525, Feb. 2021.

[37] Y. Zhao, Y. Liu, T. He, A. V. Vasilakos, and C. Hu, "FREDI: Robust RSS-based ranging with multipath effect and radio interference," in *Proc. IEEE INFOCOM*, 2013, pp. 505–509.

[38] S. Shi, Y. Xie, M. Li, A. X. Liu, and J. Zhao, "Synthesizing wider WiFi bandwidth for respiration rate monitoring in dynamic environments," in *Proc. IEEE INFOCOM*, 2019, pp. 181–189.

[39] F. Adib, Z. Kabelac, D. Katabi, and R. C. Miller, "3D tracking via body radio reflections," in *Proc. USENIX NSDI*, 2014, pp. 317–329.

[40] X. Li, S. Li, D. Zhang, J. Xiong, Y. Wang, and H. Mei, "Dynamic-music: accurate device-free indoor localization," in *Proc. ACM Ubicomp*, 2016, pp. 196–207.

[41] D. Vasisht, S. Kumar, and D. Katabi, "Decimeter-level localization with a single WiFi access point," in *Proc. USENIX NSDI*, 2016, pp. 165–178.

Yanni Yang received the BE and MSc degrees from the Ocean University of China in Qingdao, in 2014 and 2017, respectively, and the PhD degree in computer science from The Hong Kong Polytechnic University in 2021. She is currently a postdoctoral fellow with the Department of Computing, The Hong Kong Polytechnic University. She visited the Media Lab in MIT in 2019 as a visiting student. She has published papers in many conferences and journals, including, ACM Ubicomp, IEEE SECON, *IEEE/ACM Transactions on Networking*, *IEEE Transactions on Mobile Computing*, and *IEEE Internet of Things Journal.* Her research interests include wireless human sensing, pervasive and mobile computing, and Internet of Things.

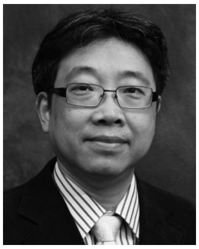

Jiannong Cao (Fellow, IEEE) received the MSc and PhD degrees in computer science from Washington State University. He is currently a chair professor with the Department of Computing, The Hong Kong Polytechnic University (PolyU). He is also the dean of Graduate School, the director of Research Institute of Artificial Intelligent of Things, the director of Internet and Mobile Computing Lab, and the vice director of University's Research Facility, Big Data Analytics, PolyU. He has coauthored five books, co-edited nine books, and authored or coauthored more than 500 papers in major international journals and conference proceedings. His research interests include distributed systems and blockchain, wireless sensing and networking, big data and machine learning, and mobile cloud and edge computing. He is a member of Academia Europaea and an ACM distinguished member.

Yanwen Wang (Member, IEEE) received the BS degree in electronic engineering from Hunan University, Changsha, China, and the MS degree in electrical engineering from the Missouri University of Science and Technology, MO, USA, in 2010 and 2013, respectively, and the PhD degree from the Department of Computing, Hong Kong Polytechnic University, Hong Kong, China, in 2020. He is currently an associate professor with the College of Electrical and Information Engineering, Hunan University, China. His research interest includes mobile and network computing, RFID systems, and acoustic sensing.